Acta Pharmacologica Sinica

www.nature.com/aps

ARTICLE

Metabolic characterization of a potent natural neuroprotective agent dendrobine in vitro and in rats

Hong Pan[1,2], Fu-guo Shi[2], Chao Fang[1] and Jing-shan Shi[2]

Dendrobine is the main sesquiterpene alkaloid of *Dendrobium nobile* Lindl, which exhibits potent neuroprotective activity. However, its metabolism and disposition are little known. In this study, we investigated the metabolic characteristics of dendrobine in vitro and in rats. The metabolic stability and temporal profile of metabolites formation of dendrobine were assayed in human/rat liver microsomal and S9 fractions. Dendrobine metabolites were separated and identified mainly by UPLC-Q/Orbitrap MS. After oral administration of dendrobine (50 mg/kg) to rats, the accumulative excretion rate of dendrobine in feces, urine, and bile was 0.27%, 0.52%, and 0.031%, respectively, and low systematic exposure of dendrobine ($AUC_{0-\infty} = 629.2 \pm 56.4$ ng·h/mL) was observed. We demonstrated that the elimination of dendrobine was very rapid in liver microsomal incubation (the in vitro elimination $t_{1/2}$ in rat and human liver microsomes was 1.35 and 5.61 min, respectively). Dendrobine underwent rapid and extensive metabolism; cytochrome P450, especially CYP3A4, CYP2B6, and CYP2C19, were mainly responsible for its metabolism. Aldehyde dehydrogenase, alcohol dehydrogenase and aldehyde oxidase were involved in the formation of carboxylic acid metabolites. By the aid of in-source fragmentation screening, hydrogen/deuterium exchange experiment, post-acquisition processing software, and available reference standards, 50 metabolites were identified and characterized in liver microsomal incubation and in rats. The major metabolic pathways of dendrobine were *N*-demethylation, *N*-oxidation, and dehydrogenation, followed by hydroxylation and glucuronidation. Collectively, the metabolic fate of dendrobine elucidated in this study not only yields benefits for its subsequent metabolism study but also facilitates to better understanding the mode of action of dendrobine and evaluating the pharmacologic efficiency of the high exposure metabolites.

Keywords: dendrobine; neuroprotective agent; drug metabolism; cytochrome P450; metabolic stability; UPLC-Q/Orbitrap MS

Acta Pharmacologica Sinica (2022) 43:1059–1071; https://doi.org/10.1038/s41401-021-00690-9

INTRODUCTION

Dendrobium nobile Lindl is a famous and valued Traditional Chinese Medicine that is recorded as a source of *Dendrobium* in Chinese Pharmacopoeia 2020 volume I [1]. Alkaloids are the major bioactive components of *Dendrobium nobile* Lindl [2]. Dendrobine is the characteristic and the most predominant alkaloid in *Dendrobium nobile* Lindl [3] and has been strongly indicated to have protective effects against the central nervous system (CNS) neurodegenerative diseases such as Alzheimer disease via the inhibition of tau protein phosphorylation, reduction of amyloid-beta deposition and induction of autophagy [4–6]. Dendrobine is deemed to be a potent natural neuroprotective agent.

Although the pharmacologic efficiency of dendrobine is widely studied, little is known about its pharmacokinetic properties and metabolic fate. It has been reported that the elimination half-life ($t_{1/2}$) of dendrobine was short (0.7 h) and the systematic exposure (AUC_{0-t}, 234 ng·h/mL) was rather low after intravenous injection of 2 mg/kg dendrobine in rats [7]. Abundant metabolites of dendrobine in rats have been reported roughly, but research elucidating their structure and the enzymes that mediate their metabolism have remained lacking [8]. Structurally, there are several potential "soft" metabolic sites, including tertiary amine, lactone and aliphatic hydrocarbon, in the structure of dendrobine. Hence, we put forward the hypothesis that the poor pharmacokinetic properties of dendrobine may be related to its extensive and rapid metabolism. The pharmacological efficacy of a drug depends on its intrinsic activity as well as the residence time and concentration in the target organ. Therefore, poor pharmacokinetic properties restrict the drug efficiency. Pharmacokinetics and metabolism studies are of great significance for the in-depth understanding of the mode of action of drugs, their active or toxic metabolites, and their safety.

In this study, the metabolic stability and the temporal profile of metabolites formation of dendrobine were assayed in incubation with human/rat liver microsomal and S9 fractions. The metabolic profiles of dendrobine were also investigated in rat bile, urine, feces, and plasma after oral administration. The metabolites were characterized mainly by ultra-high-performance liquid chromatography plus Q-Exactive Orbitrap tandem mass spectrometry (UPLC-Q/Orbitrap MS). Several other approaches including hydrogen/deuterium (H/D) exchange experiment, in-source fragmentation (ISF)

[1]Hongqiao International Institute of Medicine, Tongren Hospital and State Key Laboratory of Oncogenes and Related Genes, Department of Pharmacology and Chemical Biology, Shanghai Jiao Tong University School of Medicine, Shanghai 200025, China and [2]Key Laboratory of Basic Pharmacology of Ministry of Education & Joint International Research Laboratory of Ethnomedicine of Ministry of Education, Zunyi Medical University, Zunyi 563003, China
Correspondence: Chao Fang (fangchao32@sjtu.edu.cn) or Jing-shan Shi (shijs@zmu.edu.cn)

Received: 24 January 2021 Accepted: 28 April 2021
Published online: 28 June 2021

screening, and postacquisition processing strategies, including the multiple mass defect filter (MMDF) technique combined with Compound Discovery software and MetWorks™ Metabolite Identification Software, were comprehensively employed for metabolite identification and structure elucidation. Moreover, the multifarious metabolizing enzymes involved in dendrobine biotransformation were investigated by a special chemical inhibitor method and individual recombinant enzyme incubation.

The purposes of the present study were as follows: (1) to characterize dendrobine metabolism, including metabolic stability and metabolites, in vitro and in rats, and (2) to identify the involvement of metabolic enzymes in dendrobine biotransformation. The results help to elucidate the reason for its poor pharmacokinetic properties and to explain how dendrobine exerts its potent pharmacological efficacy in drug metabolism and disposition aspect.

MATERIALS AND METHODS

Chemicals and reagents

Dendrobine with 100% purity was obtained from Chengdu Herbpurify Co. Ltd. (Chengdu, China). *N*-demethylated dendrobine (purity 98%) and dendrobine *N*-oxide (purity 98%) reference standards were kindly provided by associate professor Mao-sheng Zhang from Zunyi Medical University. *β*-Nicotinamide adenine dinucleotide-phosphate reduced tetrasodium salt (NADPH) was purchased from Roche Diagnostic GmbH (Mannheim, Germany). Uridine 5′ diphosphoglucuronic acid trisodium salt (UDPGA), magnesium chloride ($MgCl_2$), 1-aminobenzotriazole (ABT), ticlopidine hydrochloride, and phenacetin were purchased from Sigma-Aldrich (St. Louis, MO, USA). Sulfaphenazole and disulfiram were purchased from DR. Ehrenstorfer Gmbh (Augsburg, Germany). Quinidine and ketoconazole were obtained from TCI (Shanghai, China). *α*-Naphthoflavone was obtained from Acros Organics. Formepizole, furafylline and alamethicin were purchased from Toronto Research Chemicals (Toronto, Canada). Menadione was purchased from AccuStandard (New Haven, USA). Deuterium oxide (99.8 atom % D) and 6*β*-hydroxytestosterone were obtained from J&K Scientific (Beijing, China). Methimazole and testosterone were obtained from Aladdin (Shanghai, China). Letrozole (internal standard, IS) and acetaminophen were purchased from the National Institutes for Food and Drug Control (Beijing, China). Pooled human liver microsomes (HLMs) (50 donors, equal sex mix), pooled human liver S9 (50 donors, equal sex mix) and recombinant human P450 enzymes (CYP1A2, 2B6, 2C9, 2C19, 2D6, 2E1, 3A4) were purchased from RILD Research Institute of Liver Diseases Co., Ltd (Shanghai, China). Fresh rat liver homogenates and rat liver microsomes (RLMs) were prepared from male Sprague-Dawley rats as previously described elsewhere [9, 10]. Phosphate-buffered saline (PBS, pH = 7.4, 1 M) was purchased from Beyotime Biotechnology (Shanghai, China). Methanol and acetonitrile of mass spectrometry grade were obtained from Thermo Fisher Scientific (Fair Lawn, NJ, USA). Formic acid for mass spectrometry was purchased from Honeywell Fluka (Seelze, Germany). Purified water was prepared by using a Milli-Q System (Millipore, Billerica, MA, USA).

Instrumentation and measurement conditions

The chromatographic separation and mass identification of dendrobine and its metabolites were achieved using a Thermo UltiMate3000 ultra-HPLC system interfaced with a Thermo Fisher Q/Orbitrap mass spectrometer (Thermo Fisher Scientific, Waltham, MA). Separation was conducted at 40 °C on a Thermo Scientific™ Hypersil GOLD™ C18 column (150 × 2.1 mm, 1.9 μm) with a matching Thermo Scientific™ UHPLC filter (4 mm × 2.1 mm, 0.2 μm). The UPLC mobile phases consisted of 0.1% formic acid (solvent A) and methanol (solvent B) with the optimal gradient elution programs or isocratic elution maintained at 0.3 mL/min. The gradient elution for metabolic identification was as follows: 1 min, initial 5% B; 1–5 min, 5%−20% B; 5–20 min, 20%–45% B; 20–30 min, 45%–60% B; 30–45 min, 60%–70% B; 45–47 min, 70%–90% B; 47–48 min, 90%–100% B; 48−52 min, 100% B; 52–52.5 min, 100%–5% B; and 52.5–55 min, 5% B to re-equilibrate the column. The gradient elution for the metabolic enzyme phenotyping quantification of dendrobine was as follows: 0–0.6 min, 20% B; 0.6−6.5 min, 20%−65% B; 6.5−8.5 min, 65%−90% B; 8.5−9 min, 90%−20% B; 9−12 min, 20% B. The isocratic elution for the metabolic stability study consisted of 70% A and 30% B for 4 min. The injection volume was 3 μL.

For data acquisition, MS analyses were carried out using electrospray ionization in positive ionization mode. The mass spectrometer parameters were as follows: electrospray ionization voltage at 3.5 kV, the capillary temperature at 300 °C, and aux gas heater temperature at 350 °C. The sheath gas, aux gas, and sweep gas flow rates were set to 35, 12, and 2 kV, respectively. The MS datasets were acquired using full mass/dd-MS2 mode with collision energy (CE) of 25, 30, and 38 at a scan range from *m/z* 150−650, respectively. Data analyses were carried out using Thermo Xcalibur 2.1. Compound Discoverer software Version 2.1.0.398, and MetWorks 1.3 SP4 (Thermo Fisher Scientific, San Jose, CA USA) were used as an aid to explore unknown and known metabolites and metabolic pathways.

Hydrogen/deuterium exchange experiment

The H/D exchange experiment was performed as described previously [11]. The mobile phases consisted of deuterium oxide containing 0.1% formic acid (A) and acetonitrile (B) with gradients programmed as follows: 0−0.6 min, 10% B; 0.6−6.5 min, 10%−45% B; 6.5−8.5 min, 45%−80% B; 8.5−8.8 min, 80%−10% B; 8.8−12 min, 10% B to re-equilibrate the column. The other LC-MS conditions were the same as those applied in metabolite identification. The remaining solvent in the LC system was fully washed and replaced with a deuterated mobile phase before injection of the sample. On the basis of the presence, number, and position of exchangeable hydrogen atoms, the structures of all metabolites were further elucidated.

ISF examination

The ISF of analytes was examined by screening the possible ISF products in the MS spectra of each analyte and comparing the chromatographic retention time of the ISF products with that of the parent form under different elution programs of the UPLC system. The changes in the mass response between ISF products and the parent compound were also assayed when the capillary temperature and aux gas heater temperature of the ion source were 150 °C and 150 °C, respectively [12].

In vitro metabolic stability in liver microsomal incubation

The metabolic stability of dendrobine was determined by RLM and HLM incubation at 37 °C. The reaction in the incubation system containing 1 μM of dendrobine, 1 mg/mL of liver microsomes, and 100 mM PBS (pH 7.4) was initiated by the addition of NADPH (2 mM) after 5 min of preincubation. The total incubation volume was 200 μL. The reaction was terminated at predefined time points (0, 5, 15, 30, 45, and 60 min for HLM and 0, 3, 6, 9, 15, 30, 45, and 60 min for RLM). The incubations were conducted in triplicate.

The data were calculated using a linear fit of the natural logarithm of the ratio of the dendrobine peak area to the IS peak area against time. The elimination of dendrobine can be assumed to be fitted to a first-order reaction in a certain period of time, and the well-stirred model was used to calculate in vitro metabolic stability parameters, including the elimination rate constant (*k*), elimination half-life ($t_{1/2}$), in vitro intrinsic clearance (in vitro CL_{int}), in vitro intrinsic hepatic clearance (in vitro $CL_{int\ (liver,\ in\ vivo)}$), hepatic extraction rate (E_H), and predicted in vivo clearance (in vivo CL_{int}) [13].

Metabolite identification and profiling in liver microsomal and liver S9 fractions

The in vitro metabolism assays were carried out in RLM, HLM, and rat/human liver S9 fractions. Dendrobine (10 μM) was preconditioned for 5 min at 37 °C in a mixture containing 100 mM PBS (pH 7.4) and 1 mg/mL of liver microsomes or liver S9. The total volume of incubation was 100 μL. The reaction was initiated by adding NADPH (2 mM). The reaction mixture was shaken at a constant temperature of 37 °C for 60 min. For glucuronidation incubation, a mixture containing dendrobine (10 μM), liver microsomes (1 mg/mL), alamethicin (50 μg/mL), and $MgCl_2$ (3 mM) was preincubated on ice for 15 min. Then, NADPH (2 mM) and UDPGA (5 mM) were added to the mixture and incubated at 37 °C for 60 min. Negative controls were performed in parallel, including (a) without dendrobine, (b) without NADPH, (c) without liver microsomes or S9, (d) without incubation (incubation for 0 min), and (e) without UDPGA (for glucuronidation incubation). The probe substrates of CYP3A and CYP1A, testosterone (50 μM) and phenacetin (200 μM) were incubated in parallel as positive controls. Each incubation was performed in duplicate.

Metabolizing enzymes involved in the metabolism of dendrobine

Chemical inhibitor. Selective P450 enzyme inhibitors were employed to define the role of individual P450 subfamilies in the metabolism of dendrobine in liver microsome incubation. The selective inhibitors for human P450 isoforms were ketoconazole (0.1, 1, and 10 μM) for CYP3A4, α-naphthoflavone (1 μM) for CYP1A2, sulfaphenazole (1 μM) for CYP2C9, ticlopidine (3 and 25 μM for CYP2C19 and CYP2B6), disulfiram (1 μM) for CYP2E1 and quinidine (2 μM) for CYP2D6 [14]. Different selectivity of chemical inhibitors for human P450 isoforms toward the corresponding rat P450 isoforms was reported [15]. Hence, only furafylline (1 μM, for CYP1A2), sulfaphenazole (1 μM, for CYP2C6) and ketoconazole (0.1, 1, and 10 μM, nonselective inhibitor) were used to evaluate the role of rat P450 isoforms. The nonselective P450 inhibitor ABT was also used to define the role of P450 in the metabolism of dendrobine at a final concentration of 2 mM during incubation [16]. The incubation mixtures consisted of dendrobine (1 μM), liver microsomes (1 mg/mL) and individual chemical inhibitors at various concentrations in 100 mM PBS (pH 7.4). The reactions were initiated by the addition of NADPH (2 mM) and incubated at 37 °C for 45 min (HLM) or 15 min (RLM). Ticlopidine and furafylline are the mechanism-based inhibitors, and they were preincubated for 10 min and 30 min, respectively, with liver microsomes in the presence of NADPH before the addition of dendrobine. Each incubation was performed in triplicate. Controls containing no chemical inhibitors were also included. The inhibitory effects of α-naphthoflavone (for HLM), furafylline (for RLM) and ketoconazole on the metabolism of phenacetin and testosterone were performed as positive controls. The remaining dendrobine and the production of major metabolites were monitored and quantified by UPLC-Q/Orbitrap MS to determine the contributions of the individual CYP enzymes to the metabolism of dendrobine.

Recombinant enzyme incubations. Individual recombinant human P450 enzymes were also employed to define the relative contributions of various CYP isoforms to the metabolism of dendrobine [17]. Dendrobine (1 μM) was incubated in triplicate at 37 °C for 60 min with a panel of recombinant human P450 enzymes (CYP1A2, 2B6, 2C9, 2C19, 2D6, 2E1, 3A4) at 100 pmol/mL and NADPH (2 mM) in 100 mM PBS at pH 7.4 after preincubation in the absence of NADPH. Incubations lacking NADPH were used as the control group.

The role of flavin-containing monooxygenase (FMO) in metabolism. To investigate the contribution of FMO to the metabolism of dendrobine, incubations were conducted in HLMs subjected to heat inactivation or the alternate competitive substrate inhibition by methimazole. Liver microsomes were heated at 55 °C for 1 min in the absence of NADPH for the heat inactivation of FMO. After a 5-min preincubation of control and heat-inactivated liver microsomes (1 mg protein/mL) in 100 mM PBS (pH 7.4) in the presence of NADPH (2 mM), the reaction was initiated by dendrobine (1 μM). In parallel, the normal liver microsome system was also coincubated with methimazole (500 μM). The involvement of FMO was determined by comparing control incubations with incubations where methimazole or heat inactivation was used.

Enzyme phenotyping of carboxylic acid metabolites. Fresh rat liver homogenate (25 μL) was preincubated with dendrobine (10 μM) for 5 min in 0.1 M PBS. The reactions were initiated by the addition of NADPH (2 mM) or an equal volume of PBS. The total medium volume was 100 μL. After incubation for 60 min, the reactions were quenched by cold methanol. For the inhibitor experiments, ABT (2 mM), fomepizole (a selective aldehyde dehydrogenase (ADH) inhibitor, 50 and 250 μM), disulfiram (an alcohol dehydrogenase (ALDH) inhibitor, 20, 100, and 300 μM) or menadione (a selective aldehyde oxidase (AO) inhibitor, 1 and 10 μM) was separately coincubated to identify the enzymes responsible for carboxylic acid metabolites [18, 19]. The experiments were performed in triplicate.

Animal experiment. The animal experimental procedures were conducted in accordance with the guidelines of the Institutional Animal Use and Care Committee of Zunyi Medical University. Specific pathogen-free (SPF) male Sprague Dawley rats (200−220 g) were purchased from Liaoning Changsheng Biotechnology Co., Ltd. (Certificate No. SCXK 2015-0001, Benxi, China). The rats were acclimatized for 7 d with water and food ad libitum at a temperature of 22 ± 2 °C, relative humidity of 50% ± 5%, and 12 h light and dark cycles. The rats were fasted overnight before the experiment. Dendrobine was dissolved in corn oil. The rats were randomly assigned to seven groups ($n = 3$ per group). Group 1 and Group 2 rats were orally administered dendrobine at a single dose of 50 mg/kg to collect urine, feces and bile. Group 3 rats were orally treated with ABT (100 mg/kg) for 2 d, dendrobine (50 mg/kg) was orally administered 0.5 h after the last treatment with ABT, and then the bile samples were collected. Group 4 rats received an oral dose of 50 mg/kg dendrobine, and plasma samples were collected at 0, 0.5, 1, and 4 h after treatment. The rats in the control groups (groups 5 and 6) received an equivalent volume of corn oil to collect blank bile, urine, and fecal samples. The bile samples were collected *via* bile duct cannulation with polyethylene tubing (PE-10) at the following time points: 0 (predose), 0–2, 2–4, 4–8, and 8–12 h after administration. Urine and fecal samples were collected using metabolism cages at the following intervals: 0–2, 2–4, 4–8, 8–12, 12–24, and 24–36 h. The total fecal weight and bile and urine volumes were recorded. The pharmacokinetic study was conducted in group 7. Aliquots of 100 μL blood samples were obtained from the suborbital vein and placed in heparinized tubes at 0 (predose), 0.083, 0.25, 0.5, 1, 1.5, 2, 2.5, 3, 4, 6, 8, 12, and 24 h after a single oral dose of 50 mg/kg dendrobine.

Sample preparation. All the in vitro incubation samples were prepared using the same method. That is, incubation reactions were stopped by adding three volumes of ice-cold methanol containing 50 ng/mL letrozole as an IS. Then, the samples were vortexed for 3 min and centrifuged at 13000 rpm for 10 min at 4 °C to remove the protein. The supernatant was diluted with three volumes of the mobile phase (80% water containing 0.1% formic acid and 20% methanol) and then injected into UPLC-Q/Orbitrap MS system.

Aliquot of 100 μL of urine and bile samples and 5 μL of IS solution (500 ng/mL) were precipitated with 300 μL of methanol, and then the mixtures were vortexed for 3 min and centrifuged at 13000 rpm for 10 min at 4 °C. The fecal samples at each timepoint

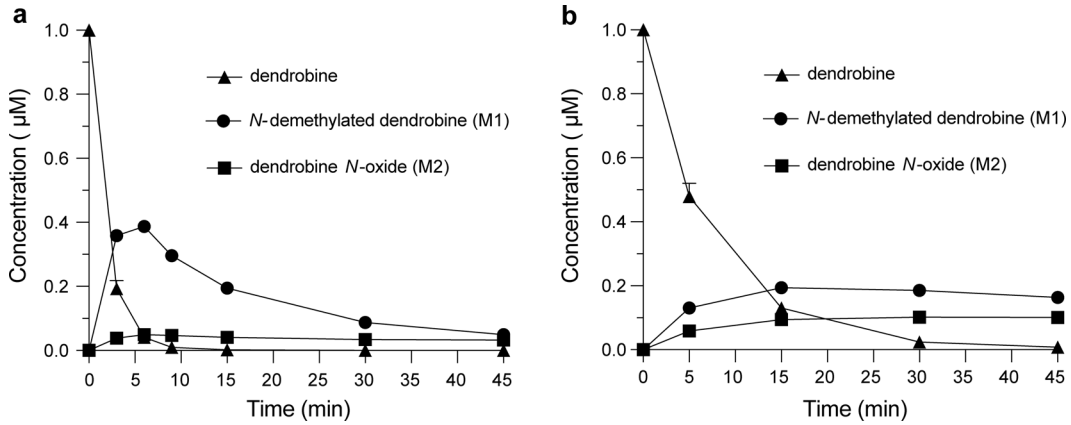

Fig. 1 The metabolic stability of dendrobine. The temporal elimination of dendrobine and formation of two major metabolites, M1 and M2, in (**a**) rat and (**b**) human liver microsomal incubation.

Table 1. Metabolic stability parameters of dendrobine calculated after incubation with liver microsomes.

Liver microsomes	k (min^{-1})	$t_{1/2}$ (min)	In vitro CL_{int} ($\mu L \cdot min^{-1} \cdot mg^{-1}$ protein)	In vitro $CL_{int\ (liver,\ in\ vivo)}$ ($mL \cdot min^{-1} \cdot kg^{-1}$)	E_H	In vivo CL_{int} ($mL \cdot min^{-1} \cdot kg^{-1}$)
Human	0.12	5.61	123.4	111.1	0.84	17.66
Rat	0.52	1.35	515.2	927.3	0.94	51.92

were dried and pulverized into powder. Weighed powder (0.1 g) was ultrasonically extracted in 0.5 mL of methanol-water (2:1, *v/v*) for 30 min. The extracted solution was centrifuged at 13,000 r/min for 10 min. The remaining protocol was similar to that of the urine and bile samples. After preparation, the bile, urine, and fecal samples were diluted 10-fold with mobile phase (95% water containing 0.1% formic acid and 5% methanol) to elucidate the metabolites. To quantify the dendrobine in the bile, urine, and fecal samples, the samples were diluted 10-, 50-, and 50-fold, respectively, with mobile phase (80% water containing 0.1% formic acid and 20% methanol) after sample preparation.

Aliquot of 20 μL plasma sample was mixed with 2 μL of IS solution (500 ng/mL) and 60 μL of methanol. The mixture was vortexed for 3 min and centrifuged at 13,000 rpm for 10 min. The supernatant was directly injected into the instrument for metabolite elucidation and quantification of dendrobine under different LC-MS conditions. All samples were frozen and maintained at −80 °C before preparation for metabolite profiling and identification.

Statistical analysis

The pharmacokinetic parameters of dendrobine were calculated *via* non-compartmental analysis of DAS (Drug and Statistics) Version 3.0 (BioGuider Corporation, Shanghai, China). The data acquired from this study are presented as mean ± standard deviation (SD).

RESULTS

Metabolic stability

The elimination of dendrobine in liver microsomal incubation was found to be very rapid. Only 0.22% dendrobine remained in RLM incubation for 15 min, and the value after 45 min in HLM incubation was 0.81% (Fig. 1). The calculated in vitro $t_{1/2}$ values were 1.35 and 5.61 min for rat and human liver microsomal incubation, respectively. As shown in Table 1, the observed in vitro C_{lint} values in rat and HLMs were 927.3 and 111.1 $mL \cdot min^{-1} kg^{-1}$, respectively. Therefore, dendrobine could be categorized as having high hepatic extraction (>0.7) [20]. The data indicated that the metabolic stability of dendrobine in liver microsomal incubation was very poor and that it may undergo rapid and extensive metabolism in vivo.

Metabolite formation in liver microsomal incubation

Three major metabolites, *N*-demethylated dendrobine, dendrobine *N*-oxide, and dehydrogenated dendrobine (metabolite identification is described below), were formed and reached a rapid peak after 6 min of incubation of 1 μM dendrobine with RLM (Fig. 1a). The concentrations of *N*-demethylated dendrobine and dendrobine *N*-oxide at 6 min were 0.39 ± 0.01 μM and 0.05 ± 0.00 μM, respectively, which were calculated from the standard curve prepared by spiking the standard reference into blank RLM. We could not provide the exact concentration of dehydrogenated dendrobine due to the lack of a reference compound. However, we roughly estimated its concentration from the standard curve of dendrobine determined by UPLC-Q/Orbitrap MS since its chemical structure was extremely similar to that of dendrobine. The value was ~0.42 ± 0.01 μM after 6 min of incubation. The residual concentration of dendrobine was 0.05 μM. Furthermore, trace amounts of other metabolites were found after 6 min of incubation (~10% of the peak area of the parent drug's mass response at 0 min). The three metabolites underwent further metabolism, such as hydroxylation, and consequently, the concentration was decreased (Fig. S1). In the positive control study, the formation rates of 6*β*-hydroxytestosterone in RLM and HLM incubation were 1782 ± 156 and 782 ± 58 $pmol(min \cdot mg)^{-1}$, respectively, and those of acetaminophen in RLM and HLM incubation were 762.6 ± 76.2 and 196.8 ± 78.3 $pmol(min \cdot mg)^{-1}$, respectively. The results indicated that the liver microsomal incubation system was useful for studying dendrobine metabolism. Similar results were observed in HLM incubation; however, the formation and elimination rates of the three major metabolites were slower than those in RLM incubation (Fig. 1b). Collectively, the data indicate that dendrobine was rapidly converted to *N*-demethylation, *N*-oxidation and dehydrogenation metabolites in liver microsomal incubation.

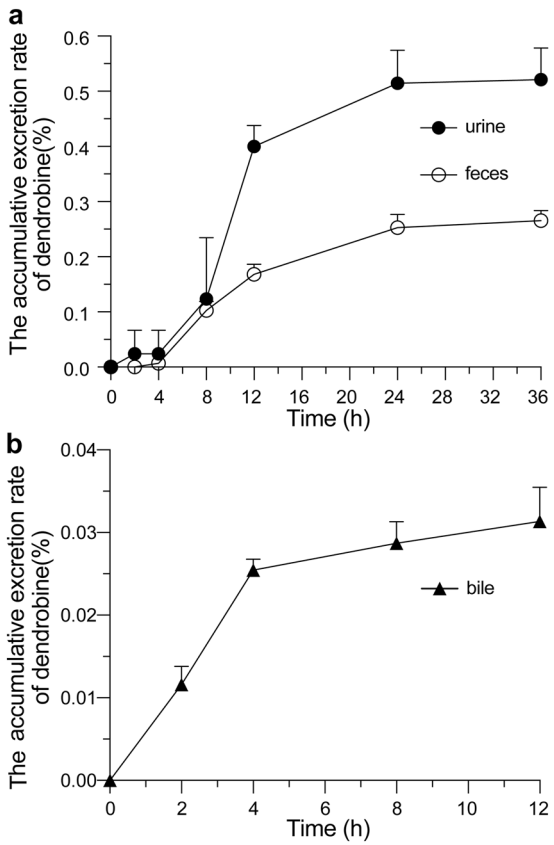

Fig. 2 Cumulative excretion of dendrobine in rats. The mean cumulative (**a**) urinary, fecal, and (**b**) biliary excretion rates of dendrobine after oral administration of 50 mg/kg dendrobine ($n = 3$).

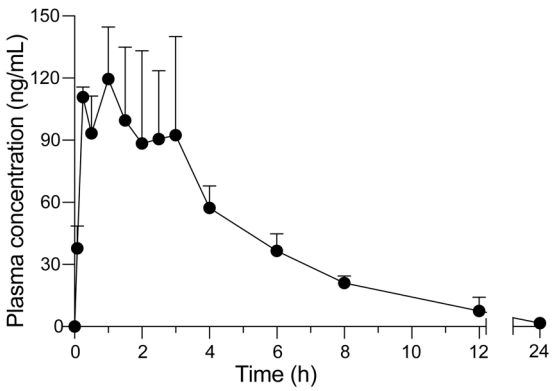

Fig. 3 The pharmacokinetics of dendrobine in rats. The mean plasma concentration-time profile of dendrobine after oral administration of 50 mg/kg dendrobine ($n = 3$).

Cumulative urinary, fecal, and biliary excretion

After the oral administration of 50 mg/kg dendrobine to rats, the cumulative urinary and fecal excretion of dendrobine for 36 h was 0.52% and 0.27%, respectively (Fig. 2a), and the cumulative biliary excretion for 12 h was 0.031% (Fig. 2b). The very low recoveries of the parent compound in urine, feces, and bile indicated that dendrobine underwent extremely extensive metabolism in rats after oral administration.

Pharmacokinetic study

The mean plasma concentration-time profile of dendrobine after a single oral dose of 50 mg/kg dendrobine is shown in Fig. 3. The multiple-peak plasma concentration phenomenon was observed. The maximum concentration (C_{max1}, C_{max2}) and time to reach C_{max} (T_{max1}, T_{max2}) were 130.0 ± 12.8 ng/mL and 107.9 ± 44.3 ng/mL and 0.92 ± 0.63 h and 3.17 ± 0.76 h, respectively. The elimination half-life ($t_{1/2}$) and mean residence time (MRT) were 3.20 ± 0.72 h and 4.75 ± 1.33 h, respectively. The area under the curve ($AUC_{0-\infty}$) was 629.2 ± 56.4 ng· h/mL. Dendrobine showed very low systemic exposure in rats after oral administration.

Metabolic profile of dendrobine in vivo and in vitro

A total of 32 and 26 metabolites of dendrobine were found in rat and human microsomal incubation, respectively. The metabolites of dendrobine generated in liver S9 fractions were closely consistent with those in liver microsomes. The predominant metabolites were *N*-demethylated, *N*-oxidative, and dehydrogenated dendrobine, which underwent further hydroxylation and glucuronidation as described above.

Totals of 43, 50, 50, and 46 metabolites were observed in rat plasma, urine, bile, and feces, respectively. In the plasma samples, M1, M3, M4, M5, M9, M10-2, M10-3, M20, and M21 were dominant metabolites according to the relative mass response. In the bile samples, the major metabolites were M1, M7-2, M9, M10-3, M11-1, M20, M21, M26-1, M29-2, and M30-3. The cumulative bile excretion rate of M1 was 3.25%, and the other major metabolites mentioned above occupied ~90% of the total peak area of all metabolites at 2-4 h postdose. In urine, the predominant metabolites were M1, M2, M5, M10-2, M10-3, M11-1, M11-2, and M26-2, which represented 75.3% of the total mass response of all metabolites during 0–24 h postdose. In feces, the major metabolites M1, M5, M7-2, M11-1, and M11-2 accounted for over 70% of the total mass response of all metabolites. Table 2 lists the characteristics of the metabolites of dendrobine in liver microsomal incubation and in rats, including their retention times, formula, main MS/MS fragments, and identification. The typical metabolic profiles in plasma and in urine, bile, and feces are shown in Fig. 4 and Fig. S3, respectively.

In summary, dendrobine undergoes extensive metabolism, and the metabolic reactions include *N*-oxidation, dehydrogenation, *N*-demethylation, mono-hydroxylation, di-hydroxylation, tri-hydroxylation, carboxylation, and glucuronidation. *N*-demethylation, *N*-oxygenation, and dehydrogenation were the initial steps in dendrobine biotransformation, followed by hydroxylation and glucuronidation (Scheme 1).

Structural elucidation of dendrobine metabolites

The metabolites were identified by analyses of their high-resolution parent ion and product ion spectra in both raw and MMDF-fileted MS/MS datasets. The Compound discovery software workflow, named Metabolism with Statistics Expected with Fish Scoring and Unknown with Pattern and Compound Class Scoring, was used to filter the potential differential substances between predose and postdose biosamples. The *N*-oxidation and hydroxylation metabolites were distinguished by the H/D exchange method. Some metabolites were validated by the available reference standards. The ISF behavior of each metabolite was examined to prevent the false identification or underestimation of metabolites since some metabolites, such as *N*-oxide or glucuronide conjugates, may fragmentize to the parent form in an ion source [21, 22]. The metabolites that underwent ISF are labeled in Table S1, and typical results of ISF examination are shown in the supplementary materials (Fig. S4). The structural elucidation of typical metabolites is described below. and the others are presented in the supplementary materials.

M0 The protonated molecule ion of dendrobine at $[M + H]^+$ *m/z* 264.1955 was found at a retention time of 12.6 min. The fragmentation behavior of dendrobine has been reported by a previous study [23]. In this study, the MS/MS dataset was acquired by a Q/Orbitrap mass spectrometer under different CE conditions.

Table 2. Identified metabolites of dendrobine in liver microsomal incubation and in rats.

Metabolic ID	Formular	RT (min)	Calculated mass (*m/z*)	Tested mass (*m/z*)	Error (ppm)	Identification	main MS/MS fragments	Source
M0	$C_{16}H_{25}NO_2$	12.6	264.1963	264.1955	−3.0	Dendrobine	218.1900, 176.1431, 145.1009, 119.0857, 70.0651,67.0549, 56.0549	–
M1	$C_{15}H_{23}NO_2$	13.7	250.1807	250.1801	−2.4	*N*-demethylated dendrobine	232.1696, 204.1747, 175.1480, 145.1012, 133.1012, 119.0857, 105.0702, 95.0859, 67.0549, 55.0550	HLM, RLM, U, F, P, B
M2	$C_{16}H_{25}NO_3$	14.4	280.1912	280.1901	−4.1	Dendrobine *N*-oxide	262.1794, 220.1327, 207.1979, 164.1432, 136.1117, 96.0810, 67.0548, 61.0402, 57.0706	HLM, RLM, U, F, P, B
M3	$C_{16}H_{23}NO_2$	9.7	262.1807	262.1797	−3.8	Dehydrogenation of M0	218.1892, 202.1571, 160.1114, 136.1119, 108.0809, 93.0701, 70.0657	HLM, RLM, U, F, P, B
M4	$C_{16}H_{23}NO_3$	20.5	278.1756	278.1755	−0.3	*N*-oxidation of M3	232.1693, 175.1482, 149.0234, 124.0759, 105.0702, 79.0548, 67.0549, 55.0550	HLM, RLM, U, F, P, B
M5	$C_{16}H_{23}NO_4$	13.1	294.1706	294.1706	0.0	Hydroxylation of M4	234.1123, 202.1227, 173.1326, 131.0856, 105.0702, 91.0549, 81.0704, 67.0549	HLM, RLM, U, F, P, B
M6-1	$C_{16}H_{23}NO_5$	6.9	310.1654	310.1649	−1.6	Hydroxylation of M5	294.1334, 232.0979, 200.1064, 161.0960, 131.0852, 110.0601, 105.0702 91.0545	U, F, P, B
M6-2		8.0		310.1648	−1.9		280.1540, 146.0267, 131.0853, 100.0217,	
M6-3		10.3		310.1651	−1.0		294.1328, 248.1278, 220.0963, 202.1218, 131.0853,119.0854, 105.0700, 93.0701, 81.0703	
M7-1	$C_{16}H_{21}NO_5$	10.8	308.1498	308.1486	−3.8	Carboxylation of M4	234.1124, 189.1151, 159.1166, 131.0856, 105.0702, 91.0547	Rat liver homogenate, U, F, P, B
M7-2		13.9		308.1479	−6.1		234.1123, 190.1223, 159.1163, 131.0856, 105.0701, 91.0545	
M8-1	$C_{16}H_{21}NO_6$	7.5	324.1447	324.1446	−0.3	Hydroxylation of M7	232.0965, 204.1016, 188.1068, 160.1115, 131.0854, 119.0856, 105.0701	U, F, P, B
M8-2		8.7		324.1445	−0.6		232.0967, 204.0652, 188.1069, 160.1117, 131.0855	
M8-3		10.5		324.1446	−0.3		232.0969, 204.1015, 185.0961, 175.1116, 159.1167, 131.0855, 121.0650, 117.0711, 91.0545	
M9	$C_{15}H_{21}NO_2$	15.1	248.1650	248.1644	−2.4	Dehydrogenation of M1	202.1590, 175.1481, 160. 1117, 119.0857, 105.0702, 93.0704, 79.0548, 67.0549, 56.0502	HLM, RLM, U, F, P, B
M10-1	$C_{15}H_{21}NO_3$	10.0	264.1599	264.1591	−3.2	Hydroxylation of M9	236.1643, 218.1542, 200.1434, 131.0856, 105.0701, 91.0547, 81.0704, 67.0549, 55.0550	HLM, RLM, U, F, P, B
M10-2		16.3		264.1595	−1.7		236.1647, 131.0856,119.0856, 93.0704, 81.0704, 67.0549, 55.0550	
M10-3		18.2		264.1588	−4.3		236.1634, 218.1538, 119.0858, 131.0856, 105.0701, 93.0703, 81.0704, 67.0549, 55.0550	
M11-1	$C_{15}H_{21}NO_4$	17.9	280.1549	280.1541	−2.9	*N*-oxidation of M10	262.1432, 245.1404, 200.1429, 131.0853, 119.0854, 105.0703, 91.0546, 81.0703, 67.0546, 55.0549	HLM, RLM, U, F, P, B
M11-2		19.4		280.1548	−0.2		147.0801, 119.0855, 105.0700, 93.0702, 81.0703	
M12	$C_{15}H_{21}NO_5$	18.5	296.1498	296.1488	−3.4	Hydroxylation of M11	236.1279, 192.1017, 172.117, 158.0966, 146.0970, 131.0858, 117.0699, 105.0698, 91.0548, 79.0549, 67.0547, 55.0551	U, F, B
M13-1	$C_{15}H_{19}NO_2$	14.3	246.1494	246.1497	−2.4	Dehydrogenation of M9	158.0963, 132.0807, 117.0547, 91.0545, 81.0704, 67.0549	HLM, RLM, U, F, B
M13-2		15.7		246.1488			158.0955, 132.0804, 117.0574, 91.0547, 81.0703	
M14	$C_{21}H_{27}NO_9$	17.9	262.1443	262.1435	0.0	*N*-oxidation of M13	243.0781, 131.0852, 119.0856, 105.0700, 91.0546, 81.0704	HLM, RLM, U, F, B
M15	$C_{15}H_{19}NO_4$	10.4	278.1392	278.1381	−4.0	Hydroxylation of M14	204.1018, 149.0231, 131.0853, 105.0700, 91.0546, 81.0706, 65.0391	HLM, RLM, U, F, P, B

Table 2. continued

Metabolic ID	Formular	RT (min)	Calculated mass (*m/z*)	Tested mass (*m/z*)	Error (ppm)	Identification	main MS/MS fragments	Source
M16-1	$C_{15}H_{19}NO_5$	9.0	294.1342	294.1340	−0.7	Hydroxylation of M15	220.0967, 159.1167, 131.0855, 105.0700, 91.0546	HLM, RLM, U, F, P, B
M16-2		11.1		294.1330	−4.1		262.1799, 220.0967, 202.0860, 174.0912, 131.0855, 109.0651, 105.0702, 93.0702	
M16-3		13.6		294.1335	−2.4		220.0967, 131.0854, 105.0701	
M17	$C_{15}H_{23}NO_3$	12.3	266.1756	266.1747	−3.4	Hydroxylation of M1	248.1648, 220.1702, 202.1590, 145.1012, 131.0857, 105.0702, 93.0703, 81.0704, 69.0705, 55.0550	HLM, RLM, U, F, P, B
M18	$C_{15}H_{23}NO_4$	18.2	282.1705	282.1699	−2.1	Hydroxylation of M17	264.1585, 222.1120, 204.1016, 131.0853, 105.0699, 81.0702	U, F, B
M19-1	$C_{16}H_{25}NO_4$	7.5	296.1862	296.1840	−7.4	Hydroxylation of M2	278.1744, 236.1275. 208.1327, 152.1066, 96.0809	HLM, RLM, U, B, P
M19-2		9.3		296.1845	−5.7		278.1737, 236.1276, 208.1330, 180.1381, 152.1071, 96.0810	
M19-3		11.2		296.1834	−9.5		278.1744, 236.1275, 208.1327, 180.1378, 152.1066, 96.0809	
M20	$C_{21}H_{31}NO_8$	22.9	426.2128	426.2110	−4.2	Glucuronidation of M1	232.1692, 204.1741, 175.1477, 145.1009, 133.1010, 119.0856, 105.0700, 67.0549, 55.0550	U, F, P, B
M21	$C_{21}H_{31}NO_9$	23.6	442.2077	442.2056	−4.7	Glucuronidation and *N*-oxidation of M1	266.1749, 250.1799, 204.1747, 175.1482, 159.1169, 145.1012, 101.0237, 83.0133, 73.0290	HLM, RLM, U, F, P, B
M22-1	$C_{21}H_{31}NO_{10}$	10.6	458.2026	458.2017	−2.0	Glucuronidation, hydroxylation and N-oxidation of M1	282.1699, 266.1747, 248.1647, 218.1537, 202.1585, 150.1729, 121.0888, 101.0237	U, F, P, B
M22-2		14.5		458.2019	−1.5		282.1697, 266.1749, 248.1634, 218.1537, 131.0855, 101.0237,	
M23	$C_{21}H_{31}NO_9$	10.5	442.2077	442.2065	−2.7	Glucuronidation of M17	266.1745, 248.1638, 218.1535	HLM, RLM, U, F, P, B
M24	$C_{22}H_{33}NO_9$	9.9	456.2233	456.2218	−3.3	Glucuronidation and hydroxylation of M0	280.1900, 117.2364, 101.0236, 73.0286	RLM, U, F, P, B
M25	$C_{22}H_{31}NO_9$	16.6	454.2077	454.2074	−0.7	Glucuronidation of M4	280.1537, 234.1483, 175.1478	U, F, B
M26-1	$C_{22}H_{31}NO_{10}$	12.9	470.2026	470.2010	−3.4	Glucuronidation of M5	294.1692, 276.1590, 234.1117, 159.0282, 131.0338, 131.0233, 85.0288,73.0289	RLM, U, F, P, B
M26-2		22.9		470.2010	−3.4		250.1798, 204.1748, 175.1483, 162.1277, 145.1014, 133.1012, 119.0857, 105.0702, 95.0859, 67.0549, 55.0548	
M27	$C_{22}H_{31}NO_{11}$	6.8	486.1985	486.1970	−3.1	Glucuronidation of M6	310.1647, 292.1540, 246.1488, 131.0340, 113.0326, 85.0289, 73.0291	U, B
M28	$C_{21}H_{29}NO_8$	11.9	424.1971	424.1955	−3.8	Glucuronidation of M9	248.1638, 231.0707, 202.1592	U, F, P, B
M29-1	$C_{21}H_{29}NO_9$	11.5	440.1920	440.1901	−4.4	Glucuronidation of M10	264.1592, 246.1487, 200.1431, 173.1325, 132.0808, 113.0236, 85.0289	RLM, U, F, P, B
M29-2		15.2		440.1948	6.3		264.1591, 248.1643, 202.1590, 175.1481, 145.1012, 121.0649, 85.0289	
M30-1	$C_{21}H_{29}NO_{10}$	10.4	456.1869	456.1858	−2.4	Glucuronidation of M11	280.1540, 262.1429, 234.1491, 189.1275, 131.0339, 113.0237, 85.0288, 73.0291	HLM, RLM, U, F, P, B
M30-2		14.3		456.1861	−1.8		280.1534, 262.1429, 234.1480	
M30-3		16.6		456.1851	−3.9		280.1537, 234.1483, 175.1479, 131.0339, 113.0236, 85.0289, 73.0290	
M31-1	$C_{21}H_{29}NO_{11}$	10.8	472.1819	472.1799	−4.2	Glucuronidation of M12	296.1483, 278.1381, 250.1436, 232.1331, 131.0852	U, F, P, B
M31-2		14.9		472.1799	−4.2		296.1484, 278.1379, 250.1434, 214.1221, 187.1121, 159.1168, 141.0178, 131.0340, 113.0233, 85.0288, 73.0289	

HLM human liver microsomes, *RLM* rat liver microsomes, *U* urine, *F* feces, *P* plasma, *B* bile.

Dendrobine was not well dissociated under low CE conditions (below 35). At the CE values ranging from 38 to 50, dendrobine produced abundant fragment ions. In general, dendrobine can be readily fragmented into lactone, isopropyl, and pyrrole ring, which were defined as ***x***, ***y***, ***z*** cleavage in this study, respectively. The diagnostic product ions at *m/z* 218.1908, *m/z* 176.1431, and *m/z* 133.1009 were produced by the successive loss of HCOOH (−46.0047 Da, cleavage ***x***), C_3H_6 (−42.0477 Da, cleavage ***y***), and $CH_2 + CH_3N$ (−43.0422 Da, cleavage ***z***). The product ions in the low *m/z* zone in the product ion spectrum were mainly generated by the cleavage of the carbon-carbon bond in the skeleton and the proposed fragmentation pathway is depicted in Fig. 5.

M1 M1 was a major metabolite of dendrobine found in liver microsomes, plasma, urine, feces, and bile samples in rats at an elution time of 13.7 min. The protonated molecule ion of M1 at $[M + H]^+$ *m/z* 250.1797 was 14.0158 Da ($-CH_2$) less than that of M0, indicating that it is a demethylation metabolite of dendrobine. The characteristic product ions at *m/z* 204.1747 and *m/z* 162.1275 derived from ***x*** and ***y*** cleavage were also 14.0154 Da less than the corresponding product ions of M0, whereas the product ions of ***z*** cleavage (*m/z* 133.1012) were the same as those of M0, which further indicated that M1 was a *N*-demethylation metabolite of dendrobine. The chemical structure of M1 was finally verified by comparing the fragmentation behavior and retention time with those of the reference standard (Fig. 6). In the H/D exchange experiment, the parent drug M0 has no exchangeable hydrogen atom deduced from a 1 Da increase in mass of the deuterated molecular ion $[M(d)+D]^+$ compared to the corresponding $[M + H]^+$. Compared with M0, the increase of 2 mass units for $[M(d) + D]^+$ of M1 indicated that an exchangeable hydrogen atom was formed by *N*-demethylation. The details of the results of the H/D exchange experiment are exhibited in Fig. S5 and Table S1 in the supplementary materials.

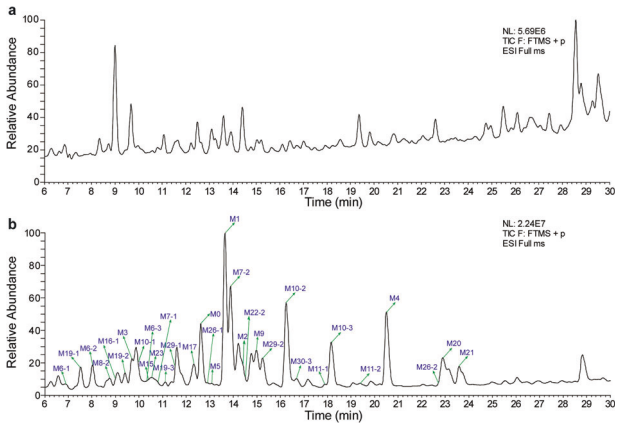

Fig. 4 Metabolic profile of dendrobine in rat plasma. (**a**) blank-control sample and (**b**) plasma sample collected 1 h after an oral administration of 50 mg/kg dendrobine detected by UPLC-Q/Orbitrap MS after MMDF filtering.

M2 M2 was a major metabolite found in liver microsomes, plasma, urine, feces, and bile samples at an elution time of 14.4 min. M2 had a protonated molecule mass of 280.1912, which is 15.9958 Da (+O) higher than that of M0. The product ions of M2 at *m/z* 262.1794, 220.1327, 192.1376 resulted from the successive neutral loss of H_2O, C_3H_6, and CO. The product ion at *m/z* 192.1376 was the ***x*** and ***y*** cleavage product of the parent ion, which underwent further loss of CH_2 and CO to generate the product ions at *m/z* 178.1219 and 164.1432. The fragment of *m/z* 192.1376 further underwent the loss of CO rather than H_2O, which supported that M2 may be an *N*-oxide metabolite of dendrobine. Importantly, M2 exhibited the same fragmentation behavior and retention time as the dendrobine *N*-oxide reference standard, which provided strong evidence that M2 is the *N*-oxide metabolite of dendrobine. No exchangeable hydrogen in the M2 structure examined by the H/D exchange study was consistent with the results of M2 structural elucidation. The product ion spectra of M2 and other typical metabolites are shown in Fig. S6 in the supplementary materials. The details of the structural elucidation of other metabolites are also given in the supplementary materials.

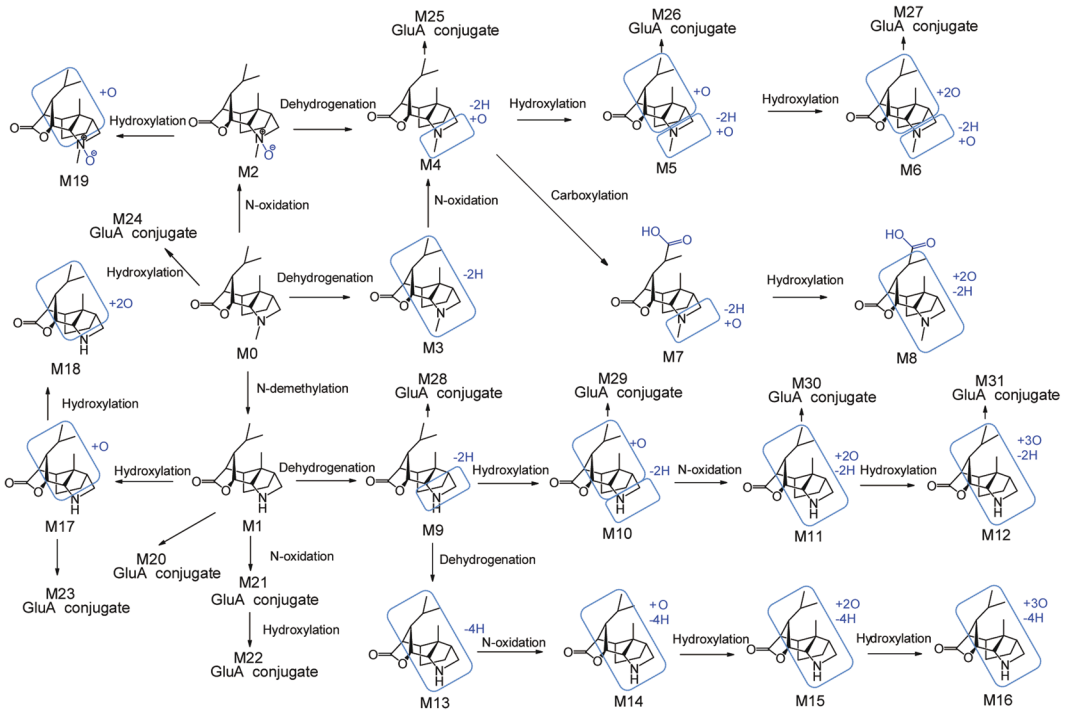

Scheme 1 Proposed metabolic pathways of dendrobine.

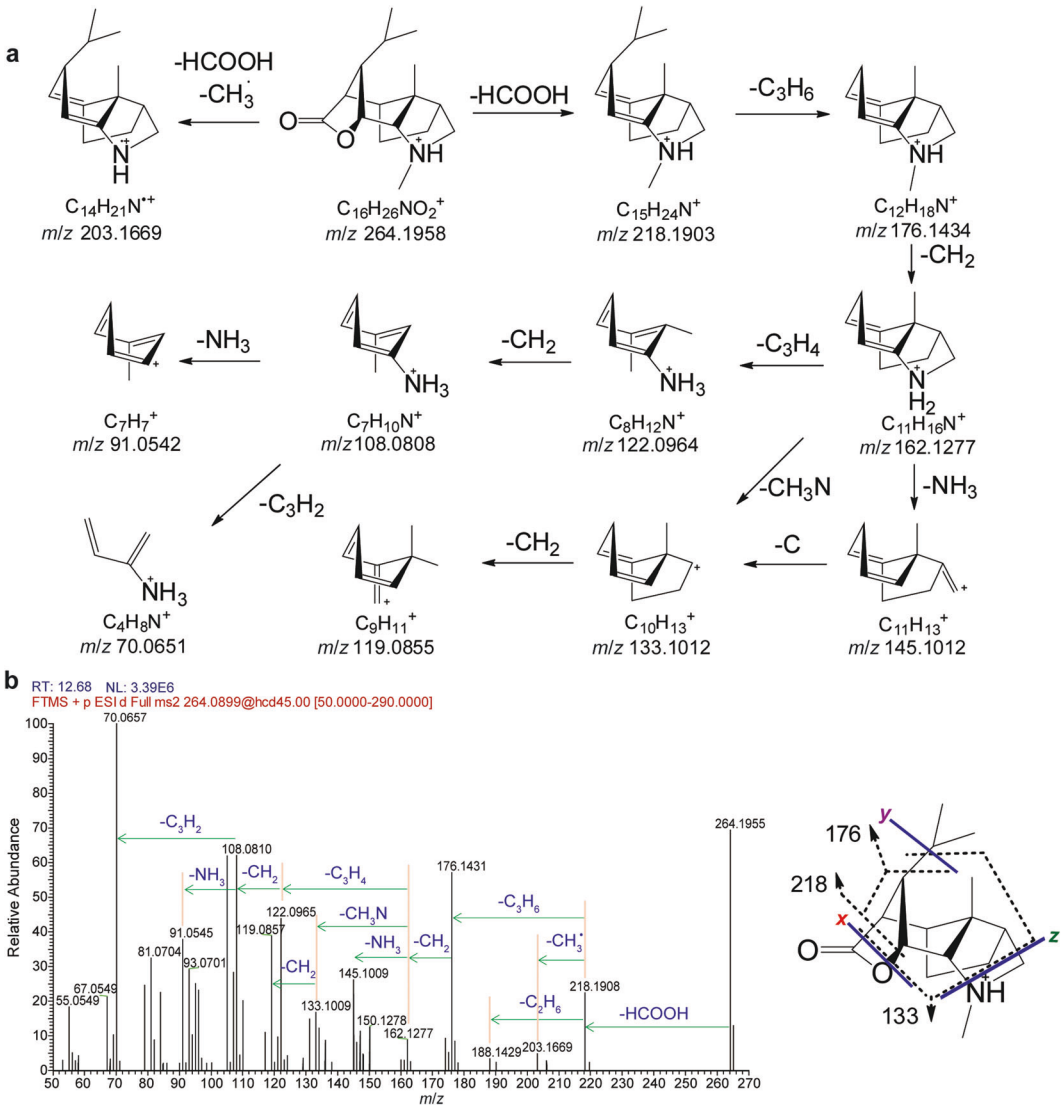

Fig. 5 The structural elucidation of dendrobine. (**a**) the proposed fragmentation pathway and (**b**) the product ion spectrum *via* UPLC-Q/Orbitrap MS.

M3–**M7** M3 was the dehydrogenated metabolite of M0. M4 was the *N*-oxide metabolite of M3. M5 was the hydroxylation metabolite of M4. M6-1, M6-2, and M6-3 were three hydroxylation metabolites of M5. M7-1 and M7-2 were two unusual carboxyl metabolites of M4 and the carboxylation metabolism site was at the isopropyl group. M8-1, M8-2, and M8-3 were three hydroxylated metabolites of M7.

M9–**M12** M9 was a dehydrogenated metabolite of *N*-demethylated dendrobine (M1). M10-1, M10-2, and M10-3 were three monohydroxylated metabolites of M9. M11-1 and M11-2 were two hydroxylation and *N*-oxide metabolites of M9. M12 was the hydroxylation metabolite of M11.

M13–**M16** M13-1 and M13-2 were two dehydrogenated metabolites of M9. M14 was the *N*-oxide metabolite of M13. M15 was a hydroxylation and *N*-oxide metabolite of M13. M16-1, M16-2, and M16-3 were three hydroxylation metabolites of M15.

M17–**M19** M17 was a hydroxylation metabolite of M1 while M18 was a dihydroxylated metabolite of M1. M19 was a hydroxylation metabolite of M2.

The metabolites from M20 to M31 were the glucuronide conjugate of the corresponding phase I metabolites, as shown in Scheme 1. M21 was the glucuronide conjugate of the *N*-oxidation metabolite of M1, whereas the unconjugated form (*N*-oxidation of M1) was not detected in any biosamples. M22 was the glucuronide conjugate of the hydroxylation and *N*-oxidation metabolite of M1, and the unconjugated form was likewise undetectable in the biosamples.

Identification of CYP enzymes involved in dendrobine metabolism

Pretreatment with the nonspecific P450 inhibitor ABT strongly inhibited metabolite formation and increased the amount of the parent compound found in rat bile samples compared to that in the dendrobine-only group (Fig. S7). The data indicated that P450 plays a critical role in the metabolism of dendrobine in rats. Individual recombinant CYP enzymes and specific P450 chemical inhibitors were employed to further define the role of P450 subfamilies in dendrobine metabolism.

In a human recombinant CYP enzyme phenotyping study, CYP3A4, CYP2B6, and CYP2C19 were the major CYP subfamilies responsible for the hepatic metabolism of dendrobine (Fig. 7a). After normalization for the relative hepatic abundance of P450 enzymes [24], the relative contributions of CYP3A4, CYP2B6 and CYP2C19 were calculated to be 64%, 24%, and 5%, respectively. For individual metabolite formation, *N*-demethylated dendrobine (M1) was mainly catalyzed by recombinant CYP2C19, followed by CYP3A4, CYP2B6, and CYP2C9. Dendrobine *N*-oxide (M2) was mainly mediated by CYP3A4. Dehydrogenated dendrobine

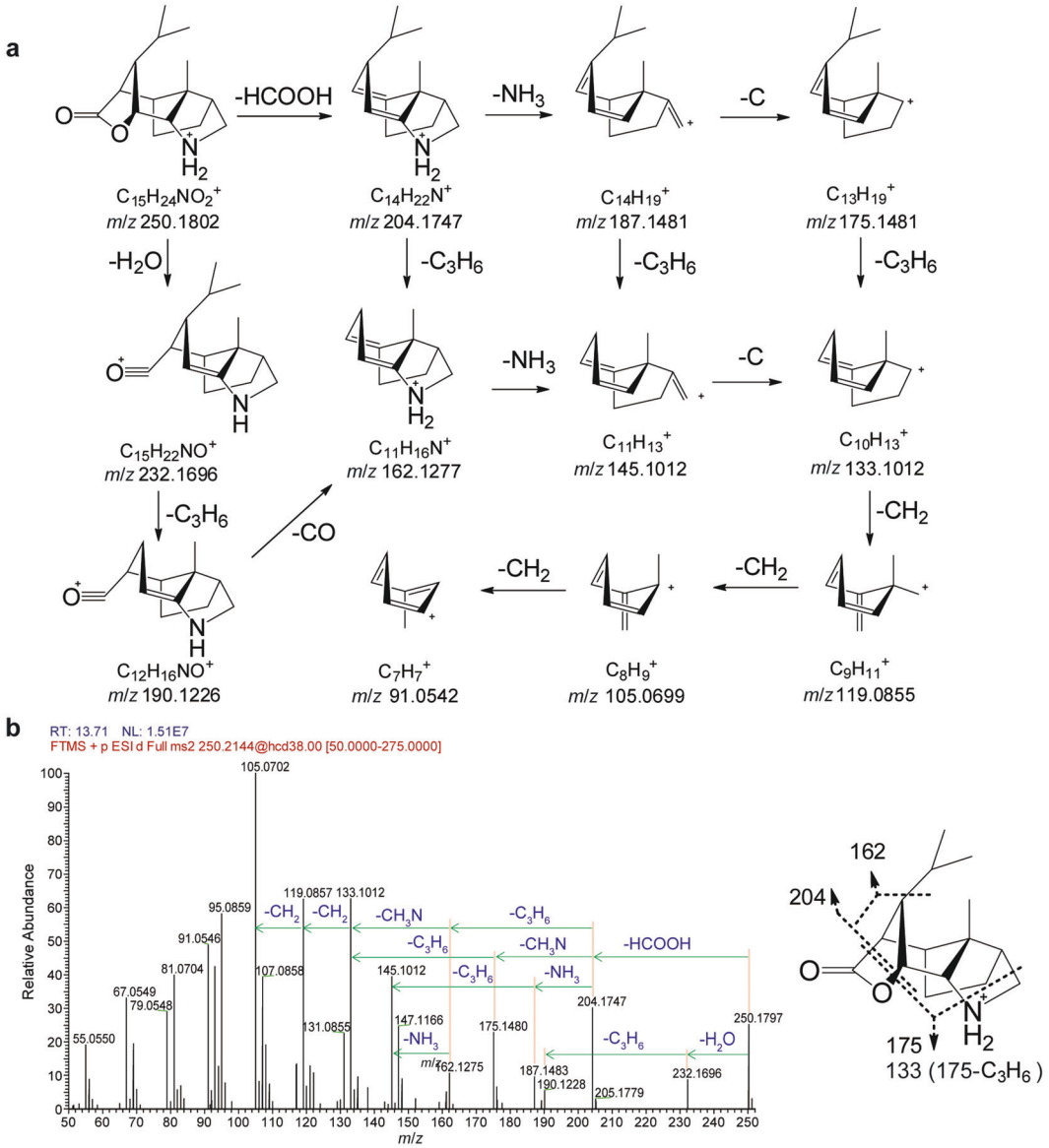

Fig. 6 The structural elucidation of *N*-demethylated dendrobine (M1). (**a**) The proposed fragmentation pathway and (**b**) the product ion spectrum *via* UPLC-Q/Orbitrap MS.

(M3) was mediated by CYP3A4 and CYP2B6 (Fig. 7b). The hydroxylation reaction was mainly catalyzed by CYP3A4 and CYP2B6 (data not shown).

The P450 enzymes involved in the metabolism of dendrobine were further confirmed by specific chemical inhibitor studies. In the positive controls, the formation of acetaminophen and 6β-hydroxytestosterone after application of the corresponding chemical inhibitors was decreased to 28.5% ± 2.5% and 15.8% ± 2.1% in RLM incubation and 35.2% ± 3.8% and 20.8% ± 5.8% in HLM incubation, respectively, compared to the control group without inhibitor. Compared with the control group, treatment with ABT powerfully inhibited the metabolism of dendrobine, indicating the predominant role of P450 in the metabolism of dendrobine in liver microsomal incubation. The metabolism of dendrobine in HLM was also strongly inhibited by the selective CYP3A inhibitor ketoconazole and somewhat inhibited by the CYP2B6/CYP2C19 inhibitor ticlopidine, as evidenced by the amounts of dendrobine remaining and the typical metabolite formation in the presence of the selective inhibitors (Fig. 7c, d). Microsome heat inactivation or methimazole inhibition did not have a marked effect on the dendrobine metabolism in HLM incubation (Fig. S8). The results suggested that FMO may have contributed to microsomal metabolism, but the contribution was very minor. The inhibition results in RLM incubation showed that ketoconazole inhibited dendrobine metabolism in a concentration-dependent manner, while furafylline and sulfaphenazole had no effect on dendrobine metabolism (data not shown). In summary, CYP enzymes played conclusive roles in the metabolism of dendrobine, and the predominant isoforms in HLM incubation were CYP3A4, followed by CYP2B6 and CYP2C19.

Metabolic enzymes involved in the formation of carboxylation metabolites

M7-1 and M7-2, proposed as carboxylic acid metabolites, were abundantly found in rat bile and feces, and their formation could be inhibited by ABT pretreatment (Fig. S7). M7-1 and M7-2 were undetectable in liver microsome incubation or liver S9 fraction incubation, whereas they could be observed in incubation with fresh rat liver homogenate. The in vitro results showed that the addition of ABT to the incubation mixture completely inhibited

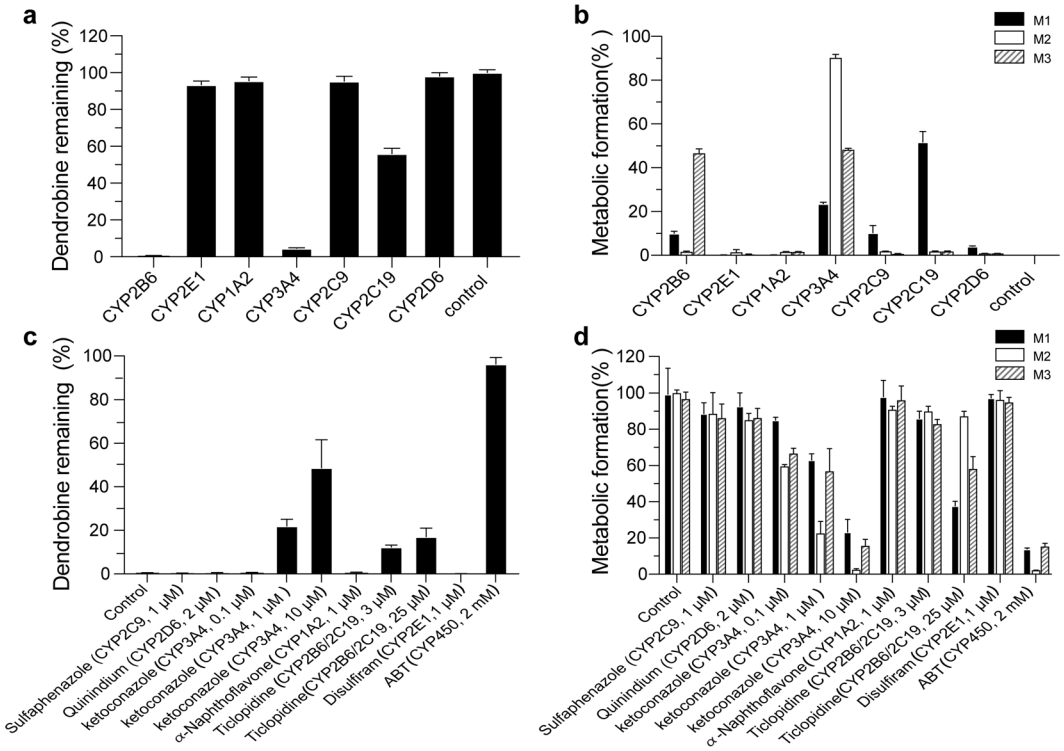

Fig. 7 The metabolism of dendrobine (1 μM) in the human recombinant P450 enzyme system. a The elimination of parent dendrobine. **b** The formation of metabolites M1, M2, and M3. Effects of P450 inhibitors on the metabolism of dendrobine in human liver microsomal incubation. **c** The elimination of dendrobine and **d** the formation of metabolites M1, M2, and M3.

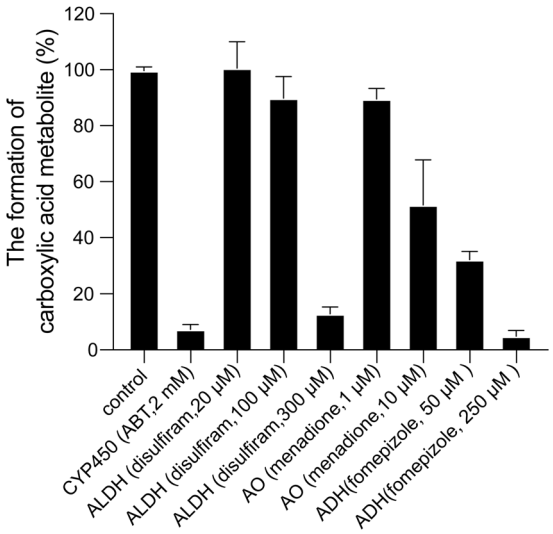

Fig. 8 The metabolic enzymes involved carboxylation metabolites formation. Effects of various metabolic enzyme inhibitors on the formation of the carboxylic acid metabolite M7-2 in NADPH-fortified rat fresh liver homogenates.

their formation. Moreover, the addition of the non-P450 oxidative enzyme inhibitors disulfiram, menadione, and fomepizole also inhibited their formation in a concentration-dependent manner. The results indicated that the two carboxylic acid metabolites were formed via dehydrogenation and *N*-oxidation followed by carboxylation. After the H/D exchange experiment, M7-1 and M7-2 had one exchangeable hydrogen atom deduced from a 2 Da mass higher than that of the corresponding $[M+H]^+$, which also supported that a carboxyl group and *N*-oxide were formed. The metabolic enzyme phenotyping was consistent with the structural characterization findings that M7-1 and M7-2 were two carboxylic acid metabolites of dendrobine after *N*-oxidation and dehydrogenation (Fig. 8).

DISCUSSION

In this study, the metabolic characteristics of dendrobine were investigated in vitro and in rats. Dendrobine was rapidly metabolized in liver microsomal incubation. The fecal, urinary, and biliary recoveries of dendrobine in rats were only 0.27%, 0.52%, and 0.031% after oral treatment with 50 mg/kg dendrobine. The dendrobine concentration in systemic circulation was much lower than that of the major metabolites, and similar patterns were observed in the plasma, fecal, urine, and bile samples. Dendrobine was not metabolized in the intestinal lumina (Fig. S9). The rapid and extensive hepatic metabolism of dendrobine seemed to be responsible for the low systemic exposure as well as extremely low fecal and urinary recoveries in vivo. The major metabolic pathways of dendrobine were *N*-demethylation, dehydrogenation, *N*-oxidation, hydroxylation, carboxylation, and subsequent hydroxylation and glucuronide conjugation. Multiple P450s, mainly CYP3A, CYP2B6, and CYP2C19, were responsible for dendrobine metabolism. In addition, some non-CYP oxidative enzymes, ALDH, AO, and ADH, contributed to the formation of carboxylic acid metabolites, two major metabolites found in rat bile and fecal samples.

Various mass spectrometric platforms were used for metabolite identification and profiling studies, which are highly dependent on the characteristic fragmentation pattern of analytes [25]. Due to the lack of characteristic fragment ions or neutral loss molecules in dendrobine, the dendrobine-related components in biological samples were carefully and artificially screened by their accurate precursor ions in MS/MS datasets and identified by MMDF-fileted MS/MS datasets. To ensure the accuracy of the identification results, the ISF behaviors of all metabolites were

examined. Several metabolites were found to undergo ISF and their ISF products may have been misdiagnosed as other metabolites when they had the same parent and product ion. For example, the glucuronide conjugate of the *N*-demethylated dendrobine (M20) was completely converted to *N*-demethylated dendrobine after in-source dissociation (Fig. S4). Furthermore, the stability of all analytes in biological samples under various conditions was examined, and they were stable during the analysis period (data not shown).

In this study, we found that dendrobine can be readily fragmented into lactone, isopropyl, and pyrrole ring, which was defined as ***x***, ***y***, ***z*** cleavage. In addition, some common fragment ions were also found to result from the cleavage of the skeleton. Therefore, the metabolites can be identified by their fragmentation behaviors according to accurate MS/MS spectra. Analyses of the mass unit changes of typical product ions cleaved from different moieties in MS/MS spectra are the common strategy to identify metabolic sites [25]. However, additional metabolic sites were not well identified in this study because the polycyclic bridged-ring system of dendrobine was not well dissociated at low CE levels, and few diagnostic product ions were cleaved from the skeleton of dendrobine at high CE levels. Another question was that the *N*-oxide and hydroxylation metabolites of dendrobine underwent the same mass unit shift (+15.9949 Da). By the aid of H/D exchange experiment, the *N*-oxide and hydroxylation metabolites as well as the conjugate site of glucuronic acid were distinguished. The identification strategy was also confirmed by available reference standards.

N-oxygenation, dehydrogenation, *N*-demethylation, hydroxylation, and glucuronide conjugation were the major metabolic pathways for dendrobine. The tertiary amine is a major active metabolic site for dendrobine, and the hydroxylation reaction may occur mainly at aliphatic hydrocarbons. The lactone ring did not undergo hydrolysis. *N*-demethylated dendrobine (M1) seems to be a predominant metabolite because its circulation concentration was 9.4- and 14.7-fold higher than that of dendrobine in rats at 0.5 and 4 h after an oral dose of dendrobine (data not shown). The data show that metabolites with high systemic concentrations may play a role in the pharmacological efficiency of dendrobine. The details of their pharmacological effects and pharmacokinetic behavior need to be further investigated in the future.

Interestingly, the study detected two unusual carboxylic acid metabolites (M7-1 and M7-2) in rats that were metabolized in the liver and then excreted into the bile and urine. It has been reported that the isopropyl can be oxidized to carboxy groups [26–28]. The formation of carboxy groups involves a wide range of metabolic enzymes [19, 29, 30]. In this study, we found that the formation of carboxylic acid metabolites was catalyzed by P450 and cytosolic enzymes, including ALDH, AO, and ADH. ADH is a family of oxidative enzyme systems that catalyze the oxidation of alcohols to corresponding aldehydes, while ALDH and AO are major oxidases in hepatic cytosols that can oxidize an aldehyde to a carboxylic acid [31]. Hence, the carboxylic acid metabolites were formed by at least three successive metabolic steps (dehydrogenation, *N*-oxidation, hydroxylation, and oxidation) in different metabolic enzyme systems.

In summary, this study demonstrated that dendrobine underwent rapid and extensive metabolism in liver microsomal incubation and in rats after oral administration. A total of 50 metabolites were identified and characterized. The major metabolic reactions were *N*-demethylation, *N*-oxidation, dehydrogenation, and the subsequent hydroxylation and glucuronide conjugation. The biotransformation of dendrobine was mediated largely by cytochrome P450 enzymes, mainly CYP3A4, CYP2B6, and CYP2C19. Cytosolic non-CYP oxidative enzymes were also involved in its metabolism. The results of this study not only explained the pharmacokinetics properties of dendrobine, but also provided a better understanding of the pharmacological efficiency of dendrobine and an evaluation of the role of the high-exposure metabolites.

ACKNOWLEDGEMENTS

This study was financially supported by the National Natural Science Foundation of China [U1812403] and the Pharmacy National First-class Discipline Construction Project of Guizhou Province of China [GNYL (2017-006)].

AUTHOR CONTRIBUTIONS

JSS and CF designed the research, directed the experiment, and performed the review and editing; HP performed the experiments, analyzed the data, and wrote the original draft. FGS performed the data analysis.

ADDITIONAL INFORMATION

Supplementary information The online version contains supplementary material available at https://doi.org/10.1038/s41401-021-00690-9.

Competing interests: The authors declare no competing interests.

REFERENCES

1. Chinese Pharmacopeia Commission, Pharmacopeia of the People's Republic of China (vol. 1). 2020 edn. China: China MedicoPharmaceutical Science & Technology; 2020.
2. Ng TB, Liu J, Wong JH, Ye X, Wing Sze SC, Tong Y, et al. Review of research on Dendrobium, a prized folk medicine. Appl Microbiol Biotechnol. 2012;93:1795–803.
3. Xu J, Han QB, Li SL, Chen XJ, Wang XN, Zhao ZZ, et al. Chemistry, bioactivity and quality control of Dendrobium, a commonly used tonic herb in traditional Chinese medicine. Phytochem Rev. 2013;12:341–36.
4. Li LS, Lu YL, Nie J, Xu YY, Zhang W, Yang WJ, et al. Dendrobium nobile Lindl alkaloid, a novel autophagy inducer, protects against axonal degeneration induced by A(25-35) in hippocampus neurons in vitro. CNS Neurosci Ther. 2017;23:329–40.
5. Nie J, Jiang LS, Zhang Y, Tian Y, Li LS, Lu YL, et al. Dendrobium nobile Lindl. alkaloids decreases the level of intracellular beta-amyloid by improving impaired autolysosomal proteolysis in APP/PS1 mice. Front Pharmacol. 2018;>9:1479.
6. Yang S, Gong QH, Wu Q, Li F, Lu YF, Shi JS. Alkaloids enriched extract from Dendrobium nobile Lindl. attenuates tau protein hyperphosphorylation and apoptosis induced by lipopolysaccharide in rat brain. Phytomedicine. 2014;21:712–6.
7. Wang SH, Wu HY, Geng PW, Lin YY, Liu ZZ, Zhang LJ, et al. Pharmacokinetic study of dendrobine in rat plasma by ultra-performance liquid chromatography tandem mass spectrometry. Biomed Chromatogr. 2016;30:1145–9.
8. Bai JQ, Guo QX, Zhang J, Huang J, Xu W, Gong L, et al. Metabolic profile of dendrobine in rats determined by ultra-high performance liquid chromatography/Quadrupole time-of-flight mass spectrometry. Comb Chem High Throughput Screen. 2020. https://doi.org/10.2174/1386207323666201023115744.
9. Shi F, Zhao P, Li X, Pan H, Ma S, Ding L. Cytotoxicity of luteolin in primary rat hepatocytes: the role of CYP3A-mediated ortho-benzoquinone metabolite formation and glutathione depletion. J Appl Toxicol. 2015;35:1372–80.
10. Bjorge SM, Baillie TA. Studies on the beta-oxidation of valproic acid in rat liver mitochondrial preparations. Drug Metab Dispos. 1991;19:823–9.
11. Penner NA, Ho G, Bercovici A, Chowdhury SK, Alton KB. Identification of two novel metabolites of SCH 486757, a nociceptin/orphanin FQ peptide receptor agonist, in humans. Drug Metab Dispos. 2010;38:2067–74.
12. Xu YF, Lu W, Rabinowitz JD. Avoiding misannotation of in-source fragmentation products as cellular metabolites in liquid chromatography-mass spectrometry-based metabolomics. Anal Chem. 2015;87:2273–81.
13. Gao ZW, Zhu YT, Yu MM, Zan B, Liu J, Zhang YF, et al. Preclinical pharmacokinetics of TPN729MA, a novel PDE5 inhibitor, and prediction of its human pharmacokinetics using a PBPK model. Acta Pharmacol Sin. 2015;36:1528–36.
14. U.S. Department of Health and Human Service, Food and Drug Administration. (2020) In Vitro Drug Interaction Studies —Cytochrome P450 Enzyme- and Transporter-Mediated Drug Interactions Guidance for Industry. http://www.fda.gov/media/134582/download (accessed January 2020).
15. Kobayashi K, Urashima K, Shimada N, Chiba K. Selectivities of human cytochrome P450 inhibitors toward rat P450 isoforms: study with cDNA-expressed systems of the rat. Drug Metab Dispos. 2003;31:833–6.
16. Tian QQ, Zhu YT, Diao XX, Zhang XL, Xu YC, Jiang XR, et al. Species differences in the CYP3A-catalyzed metabolism of TPN729, a novel PDE5 inhibitor. Acta Pharmacol Sin. 2021;42:482–90.

17. Xu Y, Zhang YF, Chen XY, Zhong DF. CYP3A4 inducer and inhibitor strongly affect the pharmacokinetics of triptolide and its derivative in rats. Acta Pharmacol Sin. 2018;39:1386–92.
18. Hou X, Zhou J, Yu S, Zhou L, Zhang Y, Zhong D, et al. Differences in the in vivo and in vitro metabolism of imrecoxib in humans: formation of the rate-limiting aldehyde intermediate. Drug Metab Dispos. 2018;46:1320–8.
19. Holm NB, Noble C, Linnet K. JWH-018 omega-OH, a shared hydroxy metabolite of the two synthetic cannabinoids JWH-018 and AM-2201, undergoes oxidation by alcohol dehydrogenase and aldehyde dehydrogenase enzymes in vitro forming the carboxylic acid metabolite. Toxicol Lett. 2016;259:35–43.
20. Salem F, Abduljalil K, Kamiyama Y, Rostami-Hodjegan A. Considering age variation when coining drugs as high versus low hepatic extraction ratio. Drug Metab Dispos. 2016;44:1099–102.
21. Jahouh F, Marongiu F, Serra MP, Laconi E, Banoub J. Gas-phase fragmentation of the N-oxide and N-hydroxylated derivatives of retrorsine using liquid chromatography/electrospray ionization quadrupole time-of-flight tandem mass spectrometry. Rapid Commun Mass Spectrom. 2015;29:1733–48.
22. Yuan L, Sophia XuX, Ji QC. Challenges and recommendations in developing LC-MS/MS bioanalytical assays of labile glucuronides and parent compounds in the presence of glucuronide metabolites. Bioanalysis. 2020;12:615–24.
23. Wang YH, Avula B, Abe N, Wei F, Wang M, Ma SC, et al. Tandem mass spectrometry for structural identification of sesquiterpene alkaloids from the stems of dendrobium nobile using LC-QToF. Planta Med. 2016;82:662–70.
24. Rodrigues AD. Integrated cytochrome P450 reaction phenotyping: attempting to bridge the gap between cDNA-expressed cytochromes P450 and native human liver microsomes. Biochem Pharmacol. 1999;57:465–80.
25. Perry SJ, Nasz S, Saeed M. A high-resolution accurate mass (HR/AM) approach to identification, profiling and characterization of in vitro nefazodone metabolites using a hybrid quadrupole Orbitrap (Q-Exactive). Rapid Commun Mass Spectrom. 2015;29:1545–55.
26. Dear GJ, Ismail IM, Mutch PJ, Plumb RS, Davies LH, Sweatman BC. Urinary metabolites of a novel quinoxaline non-nucleoside reverse transcriptase inhibitor in rabbit, mouse and human: identification of fluorine NIH shift metabolites using NMR and tandem MS. Xenobiotica. 2000;30:407–26.
27. Nomeir AA, McComish MF, Ferrala NF, Silveira D, Covey JM, Chadwick M. Liquid chromatographic analysis in mouse, dog and human plasma; stability, absorption, metabolism and pharmacokinetics of the anti-HIV agent 2-chloro-5-(2-methyl-5,6-dihydro-1,4-oxathiin-3-yl carboxamido) isopropylbenzoate (NSC 615985, UC84). J Pharm Biomed Anal. 1998;17:27–38.
28. Grabowski BA, Khosravan R, Vernillet L, Mulford DJ. Metabolism and excretion of [^{14}C] febuxostat, a novel nonpurine selective inhibitor of xanthine oxidase, in healthy male subjects. J Clin Pharmacol. 2011;51:189–201.
29. Diao X, Deng P, Xie C, Li X, Zhong D, Zhang Y, et al. Metabolism and pharmacokinetics of 3-n-butylphthalide (NBP) in humans: the role of cytochrome P450s and alcohol dehydrogenase in biotransformation. Drug Metab Dispos. 2013;41:430–44.
30. Hvenegaard MG, Bang-Andersen B, Pedersen H, Jorgensen M, Puschl A, Dalgaard L. Identification of the cytochrome P450 and other enzymes involved in the in vitro oxidative metabolism of a novel antidepressant, Lu AA21004. Drug Metab Dispos. 2012;40:1357–65.
31. Strolin Benedetti M, Whomsley R, Baltes E. Involvement of enzymes other than CYPs in the oxidative metabolism of xenobiotics. Expert Opin Drug Metab Toxicol. 2006;2:895–921.